Enhanced Magneto-Optical Effects in Epsilon-Near-Zero Indium Tin Oxide at Telecommunication Wavelengths

Kenji Ikeda,* Tianji Liu, Yasutomo Ota, Nobukiyo Kobayashi, and Satoshi Iwamoto*

Epsilon-near-zero (ENZ) materials exhibit near-zero permittivity and induce various intriguing linear and nonlinear optical phenomena. Magneto-optical (MO) effects, which are notoriously weak in the optical domain, have been predicted to be significantly enhanced in ENZ materials, which can facilitate the realization of compact nonreciprocal devices. However, to date, enhanced MO effects have been predominantly observed in effective ENZ media, which are commonly based on complex combinations of photonic nanostructures. It is difficult for these effective media to achieve isotropic ENZ responses, which severely limits their use in the development of ENZ-MO devices. Here, enhanced MO effects in pristine indium tin oxide (ITO) with ENZ properties at technologically important telecommunication wavelengths are demonstrated. MO transmission (reflection) spectroscopy of ITO films with different ENZ wavelengths reveal Faraday (Kerr) rotation peaks around the respective ENZ (EN-one) wavelengths, demonstrating that these observations are due to the intrinsic properties of the ITO materials. The demonstrated mechanism of the MO effect enhancement is universal and can be applied to various ENZ materials, including those incorporating ferromagnetic materials. Native ENZ materials with enhanced MO responses will greatly expand the opportunities for the development of novel nonreciprocal nanophotonic devices, such as on-chip optical isolators and one-way topological waveguides.

1. Introduction

Magneto-optical (MO) effects break the time-reversal symmetry and play a pivotal role in realizing nonreciprocity in photonics. MO devices are becoming increasingly important for building complex and functional optical systems that require rigorously regulated light.[1–4] At optical wavelengths, MO effects are known to be rather weak in transparent materials. Therefore, most MO devices in the optical domain require long interaction lengths and are bulky. This has been a roadblock in the development of compact optical integrated circuits with MO isolators, which are considered essential for various optical devices operating at telecommunication wavelengths, including wavelength-stabilized integrated lasers. One common approach for enhancing the effective MO interactions is to use optical resonance.[5–13] Telecom microring resonators incorporating MO materials have been examined for building compact isolators; however, they sacrifice the operational bandwidth.[14,15]

Epsilon-near-zero (ENZ) materials[16,17] represent an alternative method for increasing the effective MO interactions. ENZ media possess a relative permittivity ϵ close to zero ($-1 \leq \epsilon \leq 1$)[17] and are known to exhibit various linear and nonlinear optical phenomena, including efficient subwavelength waveguiding[18,19] and supercoupling.[19,20] Huge nonlinear optical processes in the near-infrared (NIR) region have also been observed in some ENZ media including indium tin oxide (ITO)[21] and Al-doped zinc oxide.[22] Enhanced MO effects are another anomalous aspect of ENZ materials, which have long been predicted even through a well-known equation of MO Faraday rotation found in textbooks:[23] the small diagonal part of the ϵ tensor will

K. Ikeda, N. Kobayashi
Research Institute for Electromagnetic Materials
9-5-1, Narita, Tomiya, Miyagi 981–3341, Japan
E-mail: ikeda@denjiken.ne.jp

T. Liu
GPL Photonics Laboratory
State Key Laboratory of Luminescence and Applications
Changchun Institute of Optics
Fine Mechanics and Physics
Chinese Academy of Sciences
77 Yingkou Road, Changchun, Jilin 130033, China

Y. Ota
Department of Applied Physics and Physico-Informatics
Keio University
3-14-1, Hiyoshi, Kohoku-ku, Yokohama, Kanagawa 223–8522, Japan

S. Iwamoto
Research Center for Advanced Science and Technology
Institute for Nano Quantum Information, Electronics and Institute of Industrial Science
The University of Tokyo
4-6-1, Komaba, Meguro-ku, Tokyo 153–8505, Japan
E-mail: iwamoto@iis.u-tokyo.ac.jp

ADVANCED
SCIENCE NEWS
www.advancedsciencenews.com

ADVANCED
OPTICAL
MATERIALS
www.advopticalmat.de

enhance the MO Faraday rotation, which is governed by the off-diagonal part of ϵ. In early studies, ENZ-enhanced Faraday/Kerr rotation and circular dichroism were studied theoretically.[24–26] Optical devices such as optical isolators[25] and topological one-way waveguides[27] have also been designed based on the hypothetical ENZ-MO materials.

Experimental studies on ENZ-MO media in the NIR region have mostly been conducted using effective ENZ materials based on optical metastructures.[28–30] Enhanced MO effects have been observed in effective ENZ media based on judiciously designed periodic nanostructures or complex combinations of metals and dielectric materials. Such effective media are composed of assemblies of nanophotonic elements, each of which occupies a space comparable to or even larger than the wavelength scale, exhibiting effective ENZ properties as a whole. Moreover, the optical responses of such effective media are likely anisotropic.[28–30] Combined with the difficulty in nanofabrication, it is difficult to employ nanostructure-based ENZ media for the development of ENZ-MO devices. To unleash the potential of ENZ-MO media, isotropic and continuous ENZ materials capable of enhancing the MO effects are indispensable. However, there have been no reports on enhanced MO effects in continuous ENZ media at technologically important telecommunication wavelengths.

In this study, we demonstrated that ITO thin films exhibit ENZ-enhanced MO effects at telecommunication wavelengths. We prepared ITO films with different ENZ wavelengths in the near-infrared range by controlling the oxygen concentration. We experimentally observed that the Faraday rotation and Kerr rotation in the ITO films are enhanced at around their ENZ wavelength and around the epsilon-near-one (EN-one) wavelength, respectively. Such an ENZ-enhanced MO effect would not be limited only to ITO, but would also be observed in other transparent conducting oxides exhibiting ENZ properties. The peak Faraday and Kerr rotation angles were 0.19°/μm and 0.65° at a magnetic field strength of 800 kAm^{-1}, which are surprisingly large values given that ITO is a paramagnetic material. We envision that the MO effect can be further enhanced by incorporating ferromagnetic nanogranules.[31] Our results contribute to the progress in ENZ photonics and pave the way for novel applications of ENZ materials.

2. Results and Discussion

2.1. Effect of Diagonal Element of Permittivity Tensor on MO Effects

Figure 1a shows a conceptual schematic of the experimental configuration. A magnetic field H was applied perpendicular to the specimen (Faraday configuration). When the specimen exhibited an MO response, the polarization plane of the incident light, which was linearly polarized, was rotated after being transmitted through or reflected by the specimen. The rotation angles of the polarization plane in the transmission and reflection are referred to as the Faraday rotation angle θ_F and Kerr rotation angle θ_K, respectively. The permittivity tensor of the specimen under a magnetic field along the z-direction can be expressed as:

$$\varepsilon = \begin{pmatrix} \epsilon_{xx} & \epsilon_{xy} & 0 \\ -\epsilon_{xy} & \epsilon_{xx} & 0 \\ 0 & 0 & \epsilon_{xx} \end{pmatrix} \tag{1}$$

Notably, both ϵ_{xx} and ϵ_{xy} are generally complex. When ϵ_{xy} is sufficiently smaller than ϵ_{xx}, which is the case for ordinary materials, θ_F and θ_K are approximately obtained as follows:[23]

$$\theta_F = Re\left(\frac{\pi L}{\lambda} \frac{i\epsilon_{xy}}{\sqrt{\epsilon_{xx}}} \right) \tag{2}$$

$$\theta_K = Re\left(\frac{\epsilon_{xy}}{(\epsilon_{xx}-1)\sqrt{\epsilon_{xx}}} \right) \tag{3}$$

Here, λ and L are the wavelength of the incident light and sample thickness, respectively. These results suggest that θ_F and θ_K will increase as the diagonal element of the permittivity tensor approaches zero. In addition, Equation (3) indicates that θ_K will also be enhanced when the diagonal element is close to 1. For a material with a permittivity tensor represented by Equation (1), the complex refractive indexes for the left-handed and right-handed circularly polarized light, $N_\pm$, are calculated as:

$$N_\pm = \sqrt{\epsilon_{xx} \pm i\epsilon_{xy}} \tag{4}$$

The difference between N_+ and N_- causes the rotation of the polarization plane. For the simple configuration shown in Figure 1a, neglecting the effect of the substrate, the Faraday rotation angle is calculated as follows:

$$\theta_F = Re\left\{ \frac{\pi L}{\lambda} \left(N_+ - N_- \right) \right\} \tag{5}$$

The amplitude reflectivity at the sample surface, $\tilde{r}_\pm$, is represented as:

$$\tilde{r}_\pm = \frac{N_\pm - 1}{N_\pm + 1} = r_\pm^0 e^{i\theta_\pm} \tag{6}$$

where $r_\pm^0$ and $\theta_\pm$ are real numbers. The Kerr rotation angle is then given by:

$$\theta_K = \frac{\theta_+ - \theta_-}{2} \tag{7}$$

Figure 1b,c show θ_F/L and θ_K calculated using Equations (5) and (7), as a function of the real part of ϵ_{xx}, Re(ϵ_{xx}), respectively, for various dielectric losses (the imaginary part of ϵ_{xx}, Im(ϵ_{xx})). In the calculations, $\epsilon_{xy} = 1\times10^{-4}i$ and $\lambda = 1.55$ μm were used. As expected, the increase in θ_F at around Re(ϵ_{xx}) = 0 and in θ_K at around Re(ϵ_{xx}) = 0 and 1 are clearly observed. These results show that MO effects can be effectively enhanced by controlling Re(ϵ_{xx}) at the operating wavelength. Another important observation is that the enhancement in the rotation angle becomes less prominent when the dielectric loss increases. Figure 1d shows how significantly the dielectric loss weakens the enhancement in the rotation angle, indicating the importance of preparing low-loss ENZ materials to clearly observe the enhancement of the MO effects.

2.2. ITO Films for ENZ Materials at Telecommunication Wavelengths

ITO films were prepared on a quartz substrate using a radiofrequency sputtering system. **Figure 2**a shows the optical

2301320 (2 of 8)
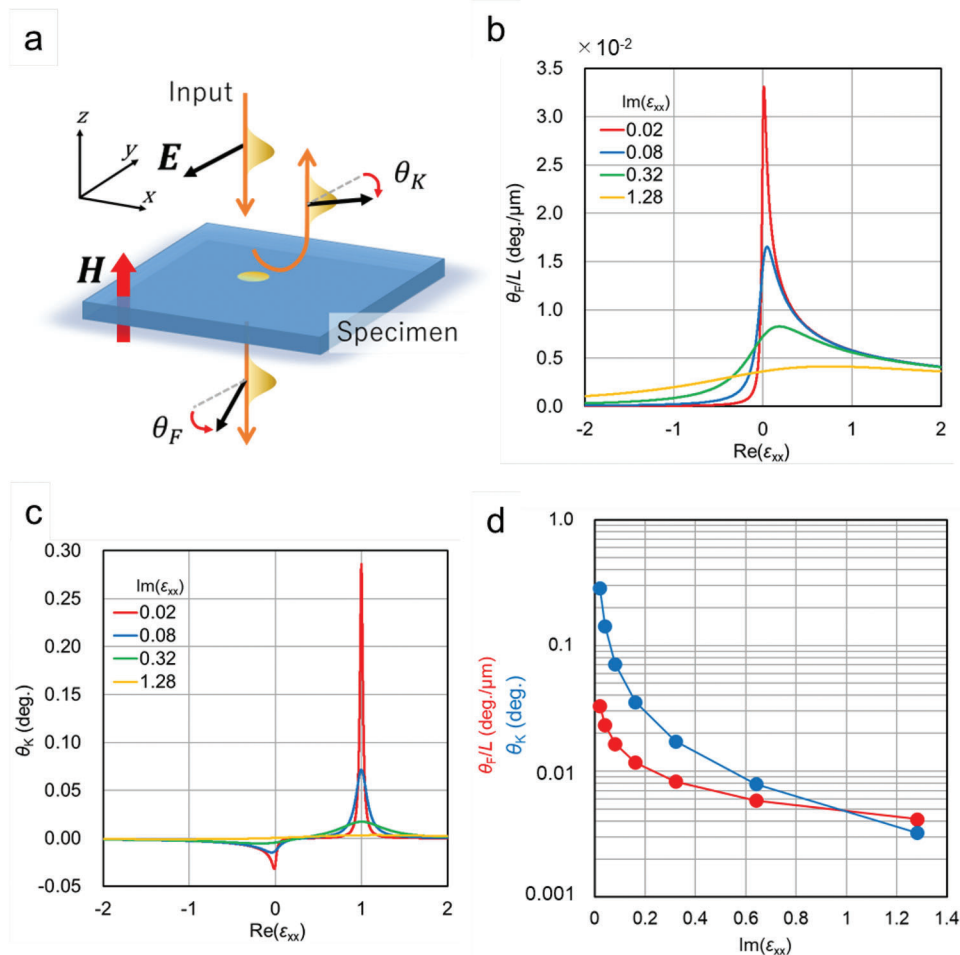
Figure 1. MO effect in an ENZ material. a) Schematic explaining MO effects in Faraday configuration. b,c) Dependences of Faraday rotation angle per length θ_F/L and Kerr rotation angle θ_K on the real part of ϵ_{xx}, Re(ϵ_{xx}), for different dielectric losses Im(ϵ_{xx}). d) Maximum Faraday and Kerr rotation angles as a function of Im(ϵ_{xx}). For the Kerr rotation angle, the peak value around Re(ϵ_{xx}) = 1 is plotted.

photographs of several ITO thin films deposited at the substrate temperature of 400 °C and with different oxygen gas flow ratios during sputtering. ITO films have visible light transmittance, and the color of the film's changes with the oxygen flow ratio. This change in color reflects the blue shift of the optical absorption edge of the ITO owing to the increase in carrier density. A lower amount of oxygen supplied during deposition increases the concentration of oxygen vacancies in the film, resulting in an increase in the carrier density.[32]

The spectra of the complex diagonal permittivity of the ITO thin films with different O_2 flow ratios are shown in Figure 2. The real part of the diagonal permittivity, Re(ϵ_{xx}), decreased and became zero at a specific wavelength depending on the O_2 flow ratio (Figure 2c). The ENZ wavelength, where Re(ϵ_{xx}) = 0, was ≈1350 nm for the ITO film deposited with O_2 flow ratio of 1%, and became longer as the O_2 flow ratio increased, exhibiting strong tunability of the ENZ wavelength covering the entire telecommunication band. The Drude model, which describes the optical response of free carriers, indicates that the ENZ wavelength depends on the plasma frequency, which is proportional to the square root of the carrier density.[33] Thus, the observed

redshift of the ENZ wavelength can be attributed to a decrease in the carrier density in the ITO films with a higher O_2 flow ratio. The carrier density of the ITO films is of the order of 10^{20} cm^{-3}, which is two orders of magnitude larger than that of highly doped InAs exhibiting ENZ-enhanced MO responses at approximately $\lambda = 17$ μm.[34] In contrast to Re(ϵ_{xx}), the imaginary part of the diagonal permittivity, Im(ϵ_{xx}), in the wavelength region of interest increases gradually as the wavelength increases owing to free-carrier absorption at longer wavelengths (Figure 2d).

As discussed above, a smaller Im(ϵ_{xx}) is desirable for investigating the ENZ-enhanced MO effects. Figure 2b shows the dielectric loss, Im(ϵ_{xx}), at the ENZ and EN-one wavelengths of the ITO films. The dielectric loss decreases as the ENZ (EN-one) wavelength decreases. This trend is consistent with that observed in previous studies (see Figure S3, Supporting Information). It is noteworthy that the dielectric losses at the ENZ wavelengths are relatively small when compared with those in previous reports, as shown in Figure S3 (Supporting Information). The low dielectric loss can be attributed mainly to high carrier mobilities owing to the high crystallinity of the ITO films deposited at a high temperature of 400 °C.
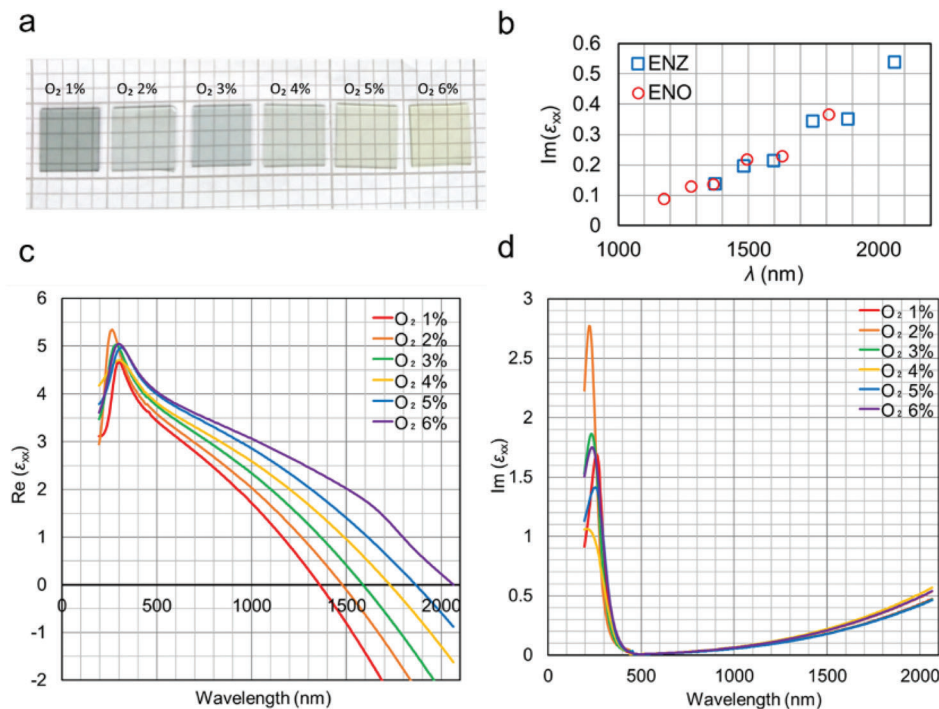
Figure 2. ITO films and their complex diagonal permittivity's. a) optical photograph of ITO films. b) Dielectric loss at ENZ and ENO wavelengths. c,d) Complex diagonal permittivity of ITO films (c, real part, d, imaginary part).
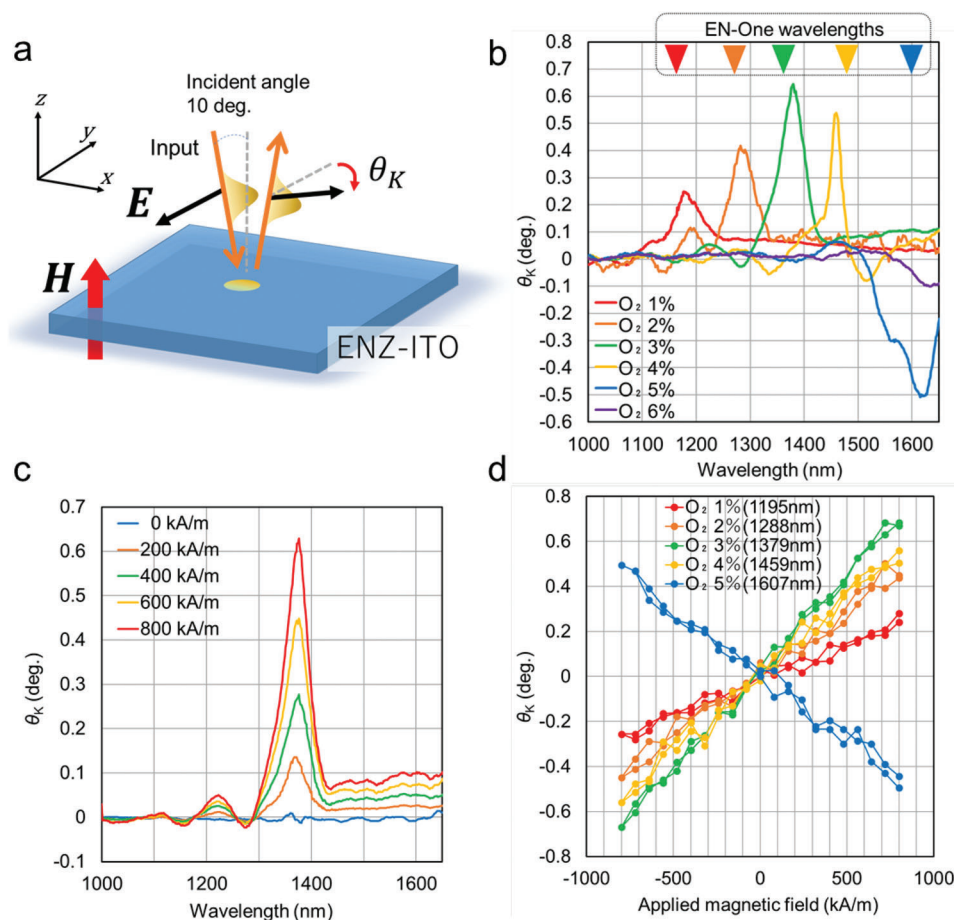
2.3. MO Effects in ENZ-ITO Films

We measured the Kerr rotation angle θ_K and Faraday rotation angle per unit length, θ_F/L, for the ITO films conforming to the Faraday geometry at room temperature. A schematic of the polar Kerr rotation measurements is shown in **Figure 3**a. In this study, the rotation angle of the polarization plane of the reflected light for S-polarized light incident at an angle of 10° was measured. Figure 3b shows the spectra of θ_K measured with a magnetic field of 800 kA m^{-1} for ITO films deposited with different O$_2$ flow ratios. As expected from Figure 1c, a peak in θ_K was observed for each sample near its EN-one wavelength, which is indicated by the arrow in Figure 3b. A corresponding peak was not observed for the film with 6% O$_2$ ratio because the EN-one wavelength was located beyond the measurement wavelength range. The sign of the peak for the ITO film with a 5% O$_2$ ratio was opposite to that of the others. Besides the main peak, we observed sub-peaks at ≈1170 and 1330 nm in ITO films with 2% and 4% O$_2$ ratios, respectively. The sign flipping and the formation of sub-peaks could be caused by the interference between the reflected lights at the ITO surface and at the interface between the ITO and quartz substrate. Besides the remarkable increase in the Kerr rotation angle at around Re(ϵ_{xx}) = 1, a slight enhancement at around Re(ϵ_{xx}) = 0 was also expected, as shown in Figure 1c. However, no clear signs of an increase in the rotation angle were observed at the ENZ wavelengths in the experiment. Because of the remaining loss, the absolute value of ϵ_{xx} was not zero, even at the ENZ wavelength, making the enhancement effect weaker and more sensitive to the loss than that at the EN-one wavelength.

Figure 3c shows the dependence of θ_K on the applied magnetic field for the ITO film deposited at an O$_2$ ratio of 3%. θ_K increases

as the magnetic field increases and reaches 0.67° at 800 kAm^{-1}. Although the rotation angle varied with the applied field, the peak wavelength of θ_K was almost independent of the magnetic field. θ_K at the peak wavelength for each ITO film is plotted as a function of the applied magnetic field in Figure 3d. θ_K varies in proportion to the magnetic field and no hysteresis is observed. These results strongly indicate that the large θ_K at the peak originates from neither the ferromagnetism of the ITO films[35] nor any other magnetic interaction enhancing the off-diagonal permittivity, but from the enhancement effect associated with the change in diagonal permittivity.

The Faraday rotation angle per unit length, θ_F/L, was measured in the transmission configuration at normal incidence under a magnetic field of 800 kAm^{-1}. **Figure 4** shows the measured θ_F/L spectra of the ITO films. In the wavelength range of interest, the free-carrier absorption in ITO increases and the transmitted optical signal weakens as the wavelength increases. The smaller the detected signal, the poorer is the signal-to-noise ratio. Therefore, θ_F/L specific to the wavelength range where the optical transmittance is larger than 1% is plotted in Figure 4 (transmittance data are shown in Figure S1a, and Faraday data for all measurement ranges are shown in Figure S2, Supporting Information, respectively). The ITO films with O$_2$ flow ratios of 1%–4% showed a broad peak. The peak wavelength shifted toward longer wavelengths as the ENZ wavelength of the films increased, but was located ≈100 nm nearer than the corresponding ENZ wavelength. For the ITO films deposited with O$_2$ flow ratio of 3%, the maximum θ_F/L of 0.19°/µm was observed at 1490 nm. The shift in the peak wavelength from the ENZ wavelength is attributed to the remaining loss. As seen in Figure 1c, Re(ϵ_{xx}), where the maximum enhancement occurred, became larger as

**ADVANCED
SCIENCE NEWS**

www.advancedsciencenews.com

**ADVANCED
OPTICAL
MATERIALS**

www.advopticalmat.de

Figure 3. Polar Kerr rotation of ENZ-ITO films. a) Schematic of the polar Kerr measurement. b) Kerr rotation spectra of ITO films. c) θ_K spectra of ITO film with O_2 deposition ratio of 3% at different magnetic fields. d) Magnetic field dependence of θ_K at the peak wavelength. θ_K in b, c and d are plotted after subtracting the Kerr rotation of the quartz substrate from the measured value.
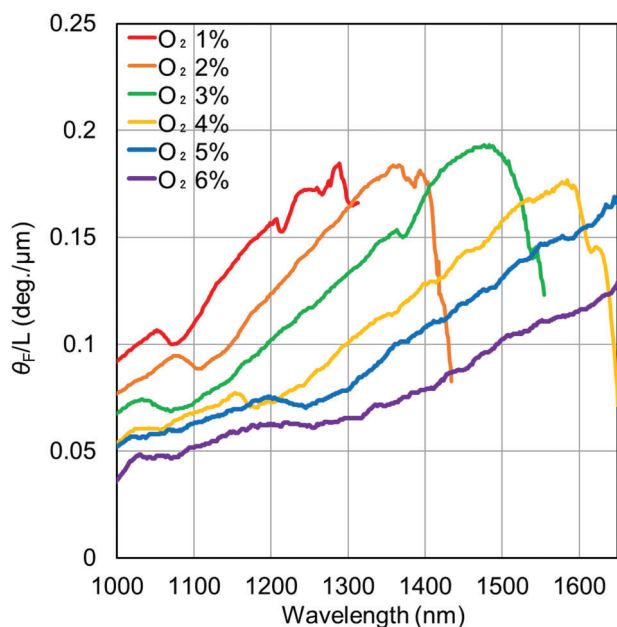

**Figure 4.** Faraday rotation angle, θ_F/L, spectra of ENZ-ITO thin films.

Im(ϵ_{xx}) increased. In addition to the shift in the ENZ wavelength, the peak shape was asymmetric. While the rotation angle gradually increased at wavelengths below the peak wavelength, it rapidly decreased above the peak wavelength. This asymmetric line shape was reasonably reproduced in the rotation spectra calculated using the measured ϵ_{xx}, as discussed below. In contrast, for the ITO films with O_2 flow ratios of 5% and 6%, only a monotonic increase in θ_F/L was observed because the expected peak wavelengths for those films were outside of our measurable spectral range.

2.4. Calculated Kerr and Faraday Rotation Spectra

To further confirm that the enhanced Kerr and Faraday rotations at particular wavelengths originated from the dispersion in the diagonal dielectric constant, we calculated the spectra of the rotation angles using the measured ϵ_{xx} shown in Figure 2c and d. **Figure 5**a and b show the calculated spectra of the Kerr rotation angle, θ_K, and Faraday rotation angle, θ_F/L, with s-polarization (along the y-direction in Figure 3a), respectively, for ITO films with different O_2 flow ratios. In the calculations, to capture the basic properties of the MO response in ITO films, we adopted
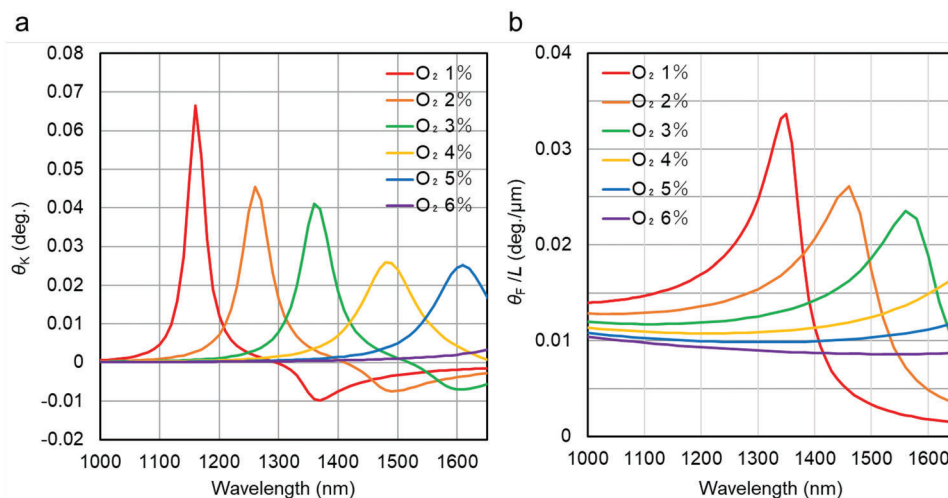
Figure 5. Faraday and Kerr rotation angles with s-polarization (out-of-plane electric field) calculated using the measured dielectric tensor. a) Kerr rotation. b) Faraday rotation.
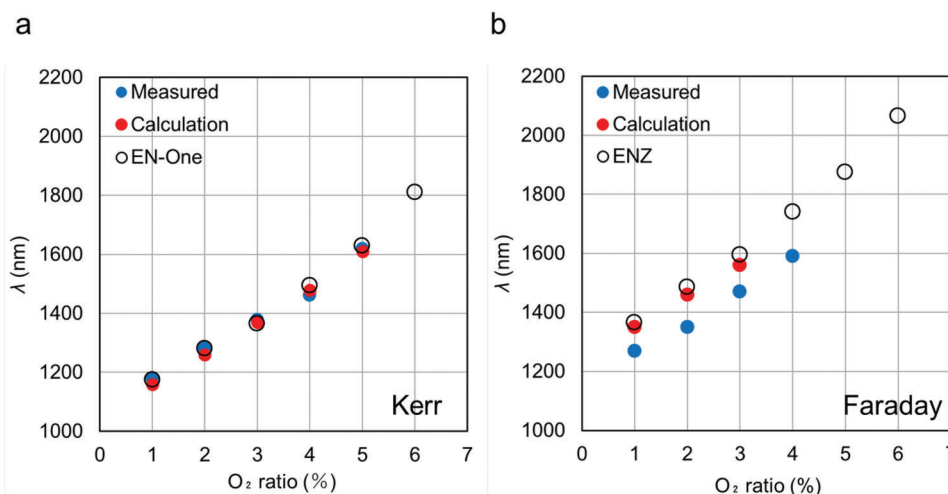
Figure 6. Measured and calculated peak wavelengths of MO effects in ITO films with different O_2 ratios. a) Peak wavelength of Kerr rotation and EN-one wavelength. b) Peak wavelength of Faraday rotation and ENZ wavelength.

a simple model assuming infinitely thick ITO films and used a fixed $\epsilon_{xy} = 1 \times 10^{-4} i$. Even this simple model can explain the fundamental features observed in the experiment, as discussed below. Incident angles of 10° and 0° were used for the Kerr and Faraday rotation calculations, respectively. The results in Figure 5 were obtained using the commercial software based on the finite element method, COMSOL Multiphysics. The modeling and calculation details can be found in Experimental Section. Calculations with fixed ϵ_{xy} reproduced the features observed in the experiments qualitatively. The main peak in the Kerr rotation spectrum appeared near the EN-one wavelength for each sample (Figure 5a). In the Faraday rotation spectra (Figure 5b), an asymmetric peak appeared, and its wavelength was a few tens of nanometers shorter than the ENZ wavelength. **Figure 6**a and b depict the measured and calculated peak wavelengths of θ_K and θ_F/L together with the EN-one or ENZ wavelengths. It can be clearly seen that the peak wavelengths in the Kerr and Faraday

rotations follow the shift in the EN-one and ENZ wavelengths, respectively. These results strongly indicate that the enhanced MO responses observed in this study are not due to the resonant enhancement of the off-diagonal permittivity but the reduced diagonal permittivity near the ENZ wavelengths.

Although the overall trend of the spectral response of the MO effect was well explained, some quantitative discrepancies remain. A major discrepancy relates to the magnitudes of the rotation angles. Both the Kerr and Faraday rotation angles measured in the experiments were five to ten times larger than those in the calculations. The electronic states at the surface differ from those in the bulk because the crystalline symmetry in the bulk is broken at the surface. This may have resulted in a larger ϵ_{xy}.[36] The optical cavity effect is another possible explanation of this phenomenon. Interference fringes were observed in the transmission and reflection spectra (Figure S1, Supporting Information), indicating the formation of optical resonance. Analysis taking the

2301320 (6 of 8)

finite thickness of ITO films will be necessary to investigate the optical cavity effect as well as the detailed features in MO spectra such as the sign and the presence of sub-peaks in the Kerr rotation spectra. In addition to the discrepancy in the rotation angles, the peak wavelengths of the Faraday rotation deviated from those in the calculations using the measured complex permittivity. This can be attributed to the variation in the optical constants of the ITO films along the thickness direction. The non-uniform composition and crystalline structure along the growth direction induce variations in the carrier density,[37] resulting in a distribution of the ENZ wavelength along the light propagation direction. Further investigations are required to clarify the origin of these discrepancies. Nevertheless, the experimental results and their qualitative agreement with the calculations presented herein (Figure 6) clearly demonstrate the enhanced MO effect in continuum ENZ materials.

3. Conclusion

In this study, we demonstrated the enhancement of the MO effect in ITO thin films exhibiting the ENZ effect at optical communication wavelengths. The low-loss ITO films exhibited an enhanced Faraday effect near the ENZ wavelength and a sharp peak of the Kerr rotation angle in the wavelength region where the dielectric constant was close to one. Enhanced MO effects can be observed in other ENZ materials, such as semiconductor oxides. The enhanced MO effects in continuum ENZ materials can be utilized to realize various integrated photonic devices, including on-chip isolators and topological one-way waveguides. We believe that our results will not only open up possibilities for new applications of ENZ materials but also contribute to further progress in ENZ photonics science.

4. Experimental Section

Materials: ENZ-ITO films were prepared using an RF sputtering system (SPF-210B, Anelva) with an ITO (Sn: 5 wt.%) target. The films were deposited on 50×50 mm quartz substrates in an $Ar + O_2$ atmosphere (O_2 ratio: 1%–6%) at a pressure of 1.0 Pa. The thickness of the films was 1.5–2.0 µm. The carrier density of the ITO films was controlled by varying the ratio of the O_2 atmosphere. The oxygen vacancies in the ITO films were varied by changing the flow ratio of the Ar and O_2 gases during deposition to fabricate films with different carrier densities.

Measurement Procedure of Diagonal Permittivity: The diagonal permittivity's of the ITO films were determined using spectroscopic ellipsometry (Uvisel Plus, Horiba) at wavelengths ranging from 200 to 2065 nm. The Lorentz and Drude models (Equations (8) and (9)) were used for the analysis of the diagonal permittivity,[33,38] wherein γ is the electron scattering rate; ϵ_0 and ϵ_∞ are the free space and infinite frequency permittivity, respectively; ω_p, ω_0, and ω are the plasma angular frequency, resonant angular frequency, and angular frequency, respectively.

$$\varepsilon_{Lorentz} = \varepsilon_\infty + \frac{\omega_p^2}{\left(\omega_0^2 - \omega^2\right) + i\gamma_L \omega} \tag{8}$$

$$\varepsilon_{Drude} = \varepsilon_\infty - \frac{\omega_p^2}{\omega(\omega + i\gamma_D)} \tag{9}$$

MO Effect Measurement: The Faraday and Kerr rotation angles were measured using the rotating analyzer method (BH-501F, Neoark) over the wavelength range of 1000–1650 nm. All the measurements were performed at room temperature.

MO Effect Calculation: All the calculations shown in Figure 5 were performed using the finite-element-method-based software package COMSOL Multiphysics. A frequency-domain solver was used to solve Maxwell's equations in a 2D model. The Floquet periodic boundary condition and scattering boundary condition were separately exploited along the x-direction and z-direction, as shown in Figure 1a. For the incident y-polarized light (s-polarization), the Faraday and Kerr rotation angles were evaluated using the following equations[23]:

$$\theta = \sigma \frac{1}{2} \frac{\arctan(2Re(\chi))}{1 - |\chi|^2}, \ \sigma = \pm 1 \tag{10}$$

$$\chi = \frac{E_x / \cos(\alpha)}{E_y} \tag{11}$$

Here, α is the incident angle in the xz-plane. E_x and E_y are the x- and y-electric field components at the reference point, respectively. σ is the sign of the rotation angles; $\sigma = -1$ and $\sigma = 1$ for θ_F and θ_K in the configuration of Figure 1a, respectively. The reference point on the transmission or reflection side was used to extract the Faraday or polar Kerr rotation angle. To calculate the Faraday rotation angle, the distance between the reference point and bottom surface of the ITO films was larger than several wavelengths. Similarly, to calculate the Kerr rotation angle, the distance between the reference point and excitation source of the film was greater than half the wavelength.

Supporting Information

Supporting Information is available from the Wiley Online Library or from the author.

Conflict of Interest

The authors declare no conflict of interest.

Data Availability Statement

The data that support the findings of this study are available from the corresponding author upon reasonable request.

[1] J. S. Krasinski, G. W. Pearson, *Acta Phys. Pol.* **1994**, *86*, 245.
[2] H. Umezawa, T. Kato, *Trans, Magn. Soc. Japan* **2004**, *4*, 330.

ADVANCED
SCIENCE NEWS

www.advancedsciencenews.com

ADVANCED
OPTICAL
MATERIALS

www.advopticalmat.de

[3] E. A. Mironov, I. L. Snetkov, A. V. Starobor, O. V. Palashov, *Appl. Phys. Lett.* **2023**, *122*, 100502.

[4] K. Srinivasan, B. J. H. Stadler, *Opt. Mater. Express* **2022**, *12*, 697.

[5] M. Inoue, K. Arai, T. Fujii, M. Abe, *J. Appl. Phys.* **1999**, *85*, 5768.

[6] T. Yoshimoto, T. Goto, R. Isogai, Y. Nakamura, H. Takagi, C. A. Ross, M. Inoue, *Opt. Express* **2016**, *24*, 8746.

[7] M. A. Kozhaev, A. I. Chernov, D. A. Sylgacheva, A. N. Shaposhnikov, A. R. Prokopov, V. N. Berzhansky, A. K. Zvezdin, I. Vladimir, *Sci. Rep.* **2018**, *8*, 11435.

[8] K. Fang, Z. Yu, V. Liu, S. Fan, *Opt. Lett.* **2011**, *36*, 4254.

[9] V. I. Belotelov, L. L. Doskolovich, A. K. Zvezdin, *Phys. Rev. Lett.* **2007**, *98*, 077401.

[10] A. B. Khanikaev, A. V. Baryshev, A. A. Fedyanin, A. B. Granovsky, M. Inoue, *Opt. Express* **2007**, *15*, 6612.

[11] A. Christofi, Y. Kawaguchi, A. Alù, A. B. Khanikaev, *Opt. Lett.* **2018**, *43*, 1838.

[12] S. Xia, S. Xia, D. O. Ignatyeva, Q. Liu, J. Qin, T. Kang, W. Yang, Y. Chen, H. Duan, L. Deng, D. Long, M. Veis, V. I. Belotelov, L. Bi, *ACS Photonics* **2022**, *9*, 1240.

[13] S. Gao, Y. Ota, F. Tian, T. Liu, S. Iwamoto, *Opt. Express* **2023**, *31*, 13672.

[14] L. Bi, J. Hu, P. Jiang, D. H. Kim, G. F. Dionne, L. C. Kimerling, C. A. Ross, *Nat. Photonics* **2011**, *5*, 758.

[15] W. Yan, Y. Yang, S. Liu, Y. Zhang, S. Xia, T. Kang, W. Yang, J. Qin, L. Deng, L. Bi, *Optica* **2020**, *7*, 1555.

[16] N. Kinsey, C. DeVault, A. Boltasseva, V. M. Shalaev, *Nat. Rev. Mater.* **2019**, *4*, 742.

[17] J. Wu, Z. T. Xie, Y. Sha, H. Y. Fu, Q. Li, *Photonics Res* **2021**, *9*, 1616.

[18] M. Silveirinha, N. Engheta, *Phys Rev Lett* **2006**, *97*, 157403.

[19] B. Edwards, A. Alù, M. E. Young, M. Silveirinha, N. Engheta, *Phys. Rev. Lett.* **2008**, *100*, 033903.

[20] Y. Li, N. Engheta, *Phys. Rev. B* **2014**, *90*, 201107(R).

[21] M. Z. Alam, I. D. Leon, R. W. Boyd, *Science* **2016**, *352*, 795.

[22] L. Caspani, R. P. M. Kaipurath, M. Clerici, M. Ferrera, T. Roger, J. Kim, N. Kinsey, M. Pietrzyk, A. Di Falco, V. M. Shalaev, A. Boltasseva, D. Faccio, *Phys. Rev. Lett.* **2016**, *116*, 233901.

[23] A. K. Zvezdin, V. A. Kotov, *Modern Magnetooptics and Magnetooptical Materials*, CRC Press, **1997**.

[24] A. R. Davoyan, A. M. Mahmoud, N. Engheta, *Opt. Express* **2013**, *21*, 3279.

[25] A. R. Davoyan, N. Engheta, *Phys Rev Lett* **2013**, *111*, 257401.

[26] Z. Guo, F. Wu, C. Xue, H. Jiang, Y. Sun, Y. Li, H. Chen, *J. Appl. Phys.* **2018**, *124*, 103104.

[27] T. Liu, N. Kobayashi, K. Ikeda, Y. Ota, S. Iwamoto, *ACS Photonics* **2022**, *9*, 1621.

[28] I. A. Kolmychek, A. R. Pomozov, A. P. Leontiev, K. S. Napolskii, T. V. Murzina, *Opt. Lett.* **2018**, *43*, 3917.

[29] I. A. Kolmychek, A. R. Pomozov, V. B. Novikov, A. P. Leontiev, K. S. Napolskii, T. V. Murzina, *Opt. Express* **2019**, *27*, 32069.

[30] I. V. Malysheva, I. A. Kolmychek, A. M. Romashkina1, A. P. Leontiev, K. S. Napolskii, T. V. Murzina, *Nanotechnol* **2021**, *32*, 305710.

[31] N. Kobayashi, K. Ikeda, B. Gu, S. Takahashi, H. Masumoto, S. Maekawa, *Sci. Rep.* **2018**, *8*, 4978.

[32] W. F. Wu, B. S. Chiou, *Semicond. Sci. Technol.* **1996**, *11*, 196.

[33] W. L. Bade, *J. Chem. Phys.* **1957**, *27*, 1280.

[34] K. J. Shayegan, B. Zhao, Y. Kim, S. Fan, H. A. Atwater, *Sci. Adv.* **2022**, *8*, eabm4308.

[35] N. H. Hong, J. Sakai, N. Poirot, V. Brizé, *Phys. Rev. B* **2006**, *73*, 132404.

[36] M. Levy, O. V. Borovkova, C. Sheidler, B. Blasiola, D. Karki, F. Jomard, M. A. Kozhaev, E. Popova, N. Keller, V. I. Belotelov, *Optica* **2019**, *6*, 642.

[37] K. S. Tseng, Y. L. Lo, *Opt. Mater. Exp.* **2014**, *4*, 43.

[38] S. Husein, M. Stuckelberger, B. West, L. Ding, F. Dauzou, M. Morales-Masis, M. Duchamp, Z. Holman, M. I. Bertoni, *J. Appl. Phys.* **2018**, *123*, 245102.